Energy- and angle-dependent threshold photoemission magnetic circular dichroism from an ultrathin Co/Pt(111) film

K. Hild,* G. Schönhense, and H. J. Elmers
Institut für Physik, Johannes Gutenberg-Universität, D-55099 Mainz, Germany

T. Nakagawa and T. Yokoyama
Institute for Molecular Science, The Graduate University for Advanced Studies (Sokendai), Myodaiji-cho, Okazaki 444-8585, Japan

K. Tarafder and P. M. Oppeneer
Department of Physics and Astronomy, Uppsala University, P.O. Box 516, S-75120 Uppsala, Sweden
(Received 24 June 2010; revised manuscript received 22 September 2010; published 15 November 2010)

Threshold photoemission magnetic circular dichroism (TPMCD) in one-photon photoemission (1PPE) and two-photon photoemission (2PPE) is measured at an ultrathin Co film grown on Pt(111). Energy-dependent measurements reveal maximum asymmetries directly at the photoemission threshold (1.90% for 1PPE and 11.7% for 2PPE) which weakly decrease with increasing photon energy. The measured TPMCD asymmetries are discussed in two excitation models on the basis of spin-resolved band-structure calculations. For the model of direct band-to-band transitions in other k directions than the direction of observation (Γ-L) *ab initio* calculations for 1PPE and 2PPE are performed. The theory is in reasonable agreement with the measured TPMCD responses. An explanation of the large 2PPE TPMCD signal is provided in terms of specific interband excitations within the first excitation step. In the case of 2PPE angle-dependent measurements reveal a continuous drop of the asymmetry with increasing angle of incidence that agrees perfectly well with a calculation using the Fresnel equations. For 1PPE a deviation from the Fresnel-field approximation is obvious.

DOI: 10.1103/PhysRevB.82.195430 PACS number(s): 71.20.−b, 75.47.−m, 75.50.Cc, 79.60.Dp

I. INTRODUCTION

Due to the interplay between the spin-orbit coupling (SOC) and the exchange interaction in ferromagnets, photoemission excited by linearly or circularly polarized light leads to an asymmetry in the spin-averaged photocurrent upon reversal of the magnetization direction. These magnetic dichroism effects have attracted much interest and developed into various experimental methods. Using synchrotron radiation, x-ray magnetic circular dichroism (XMCD) provides element specific measurements, displaying the absolute values of spin and orbital magnetic moments.[1–3] Exciting discrete atomic core levels with a large spin-orbit coupling, XMCD therefore benefits from large asymmetry values of more than 30%.[3,4] In contrast, using lasers with photon energies in the range of the sample work function, threshold photoemission magnetic circular dichroism (TPMCD) gives access to the electronic structure in the vicinity of the Fermi level E_F and thus allows insights into SOC and spin-polarization effects in bands slightly below E_F. Beyond that, magnetic imaging in threshold photoemission with maximum lateral and time resolution could be performed by using ultrashort pulse lasers with unprecedented time resolution in combination with microscopy techniques such as photoemission electron microscopy (PEEM).

Up to now there exist only few studies on threshold magnetic dichroism.[5–10] In 2000 Marx *et al.*[5] detected a magnetic linear (i.e., transversal) dichroism of 0.37% with PEEM for a 100-nm-thick polycrystalline Fe film using a mercury arc lamp. Remarkable asymmetries of $\geq$10% in one-photon threshold photoemission were found by Nakagawa and Yokoyama at perpendicularly magnetized Ni films on Cu(001) using visible and ultraviolet laser light.[6] Recently, it was shown that in the case of Ni/Cu(001) the TPMCD asymmetry is enhanced at the photoemission threshold and drops to 65% (50%) of the threshold value in the case of one-photon photoemission (1PPE) [two-photon photoemission (2PPE)] at a photon energy 0.2 eV larger than the sample work function. Moreover, angle-dependent measurements at the same sample revealed an enhanced 2PPE asymmetry at grazing incidence, which was explained by the enhancement of the electric field component normal to the surface for grazing angles.[11]

Despite these encouraging results, there is still only little knowledge about suitable thin-film systems showing large TPMCD asymmetries and the question is raised whether other systems also show an equivalent energy dependence of the TPMCD asymmetry. Otherwise, the behavior of the observed asymmetries[6,7,11] might be connected to special features in the band structure for the case of Ni/Cu(001), in particular the existence of a spin-orbit split band close to E_F at the X point.

Moreover, the asymmetry behavior for single and multiphoton-photoemission processes is a very interesting issue since it is almost not investigated up to now and would give important information about the magnitude and the general energy dependence of magnetic circular dichroism for different excitation mechanisms. Studying 1PPE would deliver gainful insights into the outright excitation of electrons from initial states slightly below the Fermi energy to final states above the vacuum level in the regime of threshold photoemission. In 2PPE the first photon excites the electron to an intermediate state and the subsequent absorption of a second photon of the same laser pulse leads to the transition

to the final state. From TPMCD measurements we can expect new information about the two excitation steps and the intermediate state involved in the 2PPE process. The angle dependence of the TPMCD asymmetry has up to now been investigated for the Ni case only and more systematics is needed to understand its origin. Especially for applications with PEEM it is of interest to examine under which conditions enlarged TPMCD asymmetries arise for grazing incidence.

Gaining more information about suitable thin-film systems, the absolute magnitude, energy dependence and angle dependence of magnetic circular dichroism for different photoemission processes would not only be interesting from the viewpoint of fundamental research but also for applications in time- and laterally resolved microscopy techniques with future investigations of magnetization dynamics in mind. The aim of the present paper is to contribute to these issues. Thereby, the main goal of this work is to explain the different asymmetry values for 1PPE and 2PPE by separate excitation mechanisms as well as to partly deduce this difference from features of the Co band-structure scheme. This information should provide an indication of different preconditions for enhanced magnetic asymmetries.

Owing to its perpendicular anisotropy, a 4.5-monolayer (ML)-thick Co film grown on Pt(111) was chosen. Co/Pt systems have attracted strong interest due to their high perpendicular magnetic anisotropy in ultrathin films and their large magneto-optical Kerr effect. Thus, they represent suitable candidates for applications in magneto-optical recording media.[12–14] Since both the exchange splitting and the spin-orbit coupling are preconditions for the appearance of magnetic circular dichroism the combination of ferromagnetic Co and Pt with a high nuclear charge Z is promising for enhanced TPMCD asymmetries.[15,16]

Despite these good preconditions, previous TPMCD measurements on a Pt/Co/Pt trilayer yielded surprisingly low asymmetries in the 0.1% range.[10] The question remained whether this small MCD was a consequence of the Pt capping layer. In the present paper we present TPMCD measurements on high-quality epitaxial Co films on Pt(111) without capping layer. Remarkable TPMCD asymmetries of up to 11.7% (2PPE) and 1.9% (1PPE) are measured directly at the threshold, which are more than one order of magnitude larger than the asymmetry values for the capped system. The results are quantitatively analyzed on the basis of spin-resolved band-structure calculations for fcc Co, performed within the framework of the local spin-density functional theory. We use direct *ab initio* calculations to explain the 1PPE TPMCD asymmetry. For the theoretical prediction of the 2PPE TPMCD we have to adopt excitation model assumptions to explain the observed, large asymmetry.

Angle-dependent measurements reveal a suprising constant behavior of the asymmetry in the case of 1PPE. For 2PPE the asymmetry decreases with increasing angle of incidence. In the framework of the Fresnel formalism this behavior is attributed to the expected loss of circular polarization in bulk material with increasing angle of incidence.

II. EXPERIMENTAL

Before deposition the Pt(111) single crystal was cleaned by Ar-ion sputtering and subsequent annealing at 670 °C.

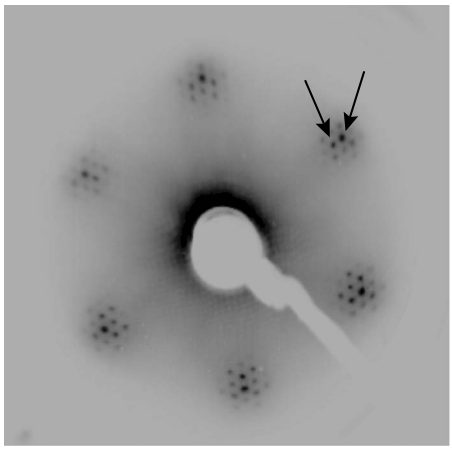

FIG. 1. LEED pattern of 4.5 ML Co/Pt(111) at 129.7 eV.

The quality of the substrate surface and the epitaxial Co film was controlled by low-energy electron diffraction (LEED). In order to prepare a sample with a large Kerr rotation, characteristic for a magnetization vector oriented out of the sample plane, a Co thickness of 4.5 ML was chosen.[10,17] The deposition was carried out at room temperature by electron-beam evaporation with a rate of 1 ML/4.5 min. Figure 1 depicts a LEED image of the Co/Pt sample at an electron energy of 129.7 eV. The sixfold symmetry of the epitaxial Co film can be clearly seen. The reflections with highest intensity correspond to the Co lattice (right arrow) while the neighboring inner reflections (left arrow) originate from the Pt substrate. Also observable is a modulation of the Co lattice reflections induced by the underlying substrate. This superstructure represents a Moiré pattern arising from regular dislocations.[18,19]

After preparation the sample was investigated by *in situ* polar magneto-optical Kerr effect (PMOKE) measurements. TPMCD asymmetries have been investigated using the same setup. Figure 2 shows a schematic drawing of the experimental setup. For the excitation of photoelectrons a broadband ultrashort pulse laser ($\tau < 100$ fs, 80 MHz repetition rate) was used with photon energies ranging from $h\nu = (5.06-5.84)$ eV for 1PPE and $h\nu = (2.46-2.92)$ eV for 2PPE. These ranges correspond to the fourth and the second harmonic of the TiSa-laser radiation. The beam was adjusted in the vacuum chamber via a system of apertures and a lens. The sample was placed between the pole shoes of an electromagnet, generating a maximum magnetic field of $\mu_0 H = 0.3$ T. Circular polarization was achieved by quarter wave plates for the particular wavelengths. By placing an anode plate (1478 V) in front of the sample the emitted photoelectrons from the perpendicularly magnetized film were measured via the sample current. To generate 2PPE processes an additional lens ($f = 15$ mm) was used in the vacuum chamber and possible admixture of one-photon photoemission processes was cut off by using an optical filter. All measurements were carried out at room temperature. During Kerr- and energy-dependent TPMCD measurements the sample was magnetically saturated along the surface normal so that the sample magnetization was oriented parallel or antiparallel to the helicity vector of the incoming laser light (see also Fig. 1 in Ref. 10)

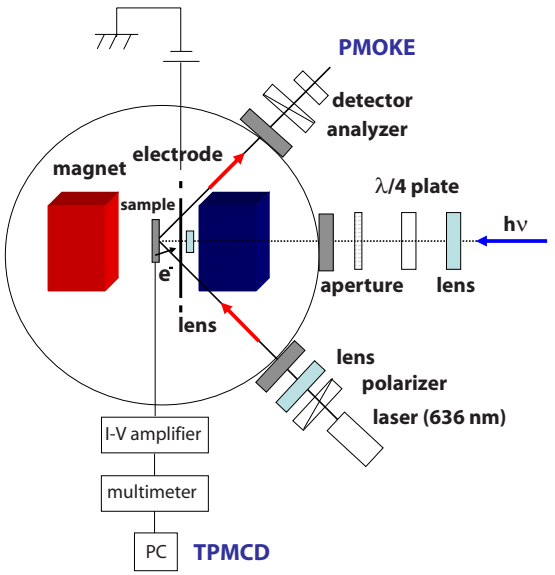

FIG. 2. (Color online) Schematic drawing of the experimental setup for Kerr and TPMCD measurements in the polar setup. Photon energy range is $h\nu$=(5.06–5.84) eV for 1PPE and (2.46–2.92) eV for 2PPE.

III. RESULTS

Polar Kerr measurements were carried out under 45° incidence of 636 nm laser light to determine the magnetic properties of the sample. Figure 3(a) depicts a Kerr measurement in polar geometry. The observed easy-axis curve (remanence equals saturation, coercive field 580 Oe) shows that the sample magnetization is oriented along the surface normal. The Kerr rotation in saturation amounts to 22.6 mdeg. Compared to the value for the Pt-capped system[10] the Kerr rotation angle is almost twice as large, revealing that the capping layer reduces the Kerr rotation.

Figure 3(b) shows a typical 1PPE TPMCD measurement. It represents an average over 30 hysteresis loops. Each hysteresis loop consists of 160 current readings. For 2PPE TPMCD 240 current readings per hysteresis loop were taken. Since all hysteresis loops reveal easy-axis magnetization curves, the TPMCD asymmetry for 1PPE as well as for 2PPE is evaluated as follows:

$$A_{\mathrm{TPMCD}} = \frac{\overline{I_S}^{M^+} - \overline{I_S}^{M^-}}{\overline{I_S}^{M^+} + \overline{I_S}^{M^-}}, \tag{1}$$

where $\overline{I_S}^{M^+}$ ($\overline{I_S}^{M^-}$) are the averaged values of the sample currents for positive (negative) sample magnetization direction, measured for a fixed photon helicity. Alternatively, the magnetization can be fixed and the photon helicity be reversed. In each measurement we ensured that a reversal of the photon helicity led to a reversal of A_{TPMCD} as described in Ref. 8.

In order to determine the sample work function the dependence of the electron yield on the photon energy was measured in the range (5.06–5.84) eV. This dependence is plotted in Fig. 4. The electron yield is defined as: $N=\frac{I_S h\nu}{Pe}$, where N is the number of electrons, I_S is the sample current, $h\nu$ is the photon energy, P is the power of the laser beam, and e is the elementary charge. For an energy difference ≤ 1 eV between the photon energy and the sample work function a linear relation between the electron yield and the photon energy is found. For photon energies smaller than the sample work function the electron yield approaches almost zero. A linear

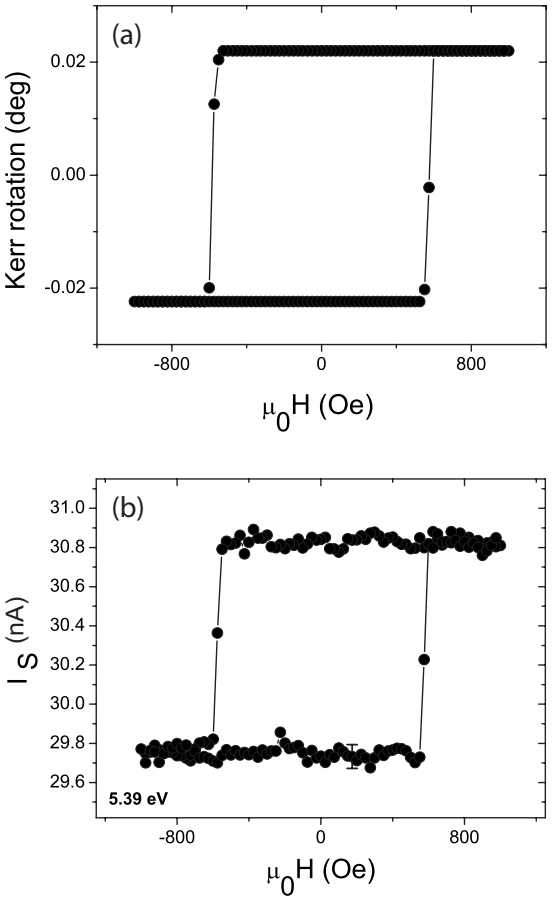

FIG. 3. (a) Polar Kerr measurement. The error bars are on the order of the symbol size. (b) Drift-corrected 1PPE TPMCD measurement showing the sample current at a photon energy of 5.39 eV. The figure represents an average over 30 hysteresis loops, each hysteresis loop consists of 160 current readings. A typical error bar is shown on the bottom branch.

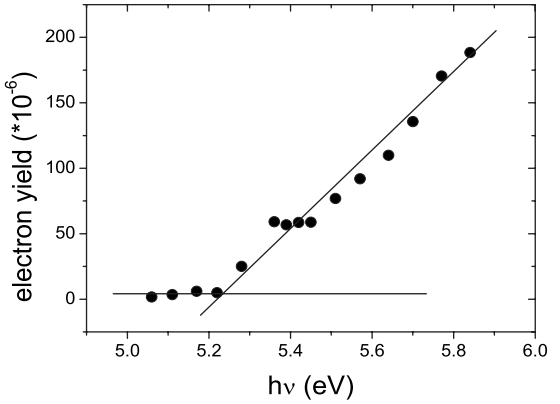

FIG. 4. Dependence of the electron yield on the photon energy for the determination of the sample work function.

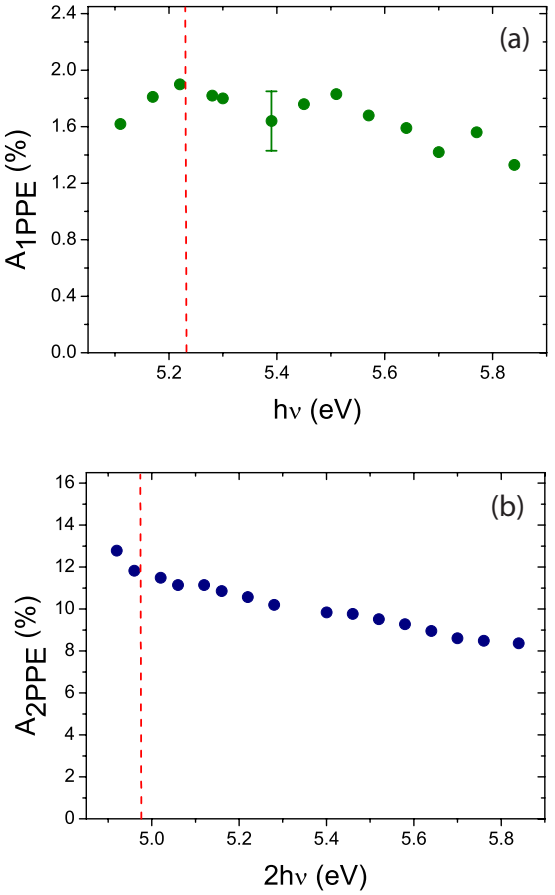

FIG. 5. (Color online) (a) Energy dependence of the 1PPE TPMCD asymmetry for 4.5 ML Co/Pt(111). (b) Same for the 2PPE TPMCD asymmetry. The dashed lines mark the photoemission thresholds determined from work-function measurements. All measurements were carried out in the polar Kerr setup. For 1PPE a characteristic error bar has been derived that is mainly due to statistical fluctuations of the measured data. For 2PPE the error bars are in the order of the symbol size because of the larger absolute asymmetry values.

fit determines the work function to $\Phi=(5.23\pm0.1)$ eV in the case of 1PPE. The determination of the work function prior to the 2PPE measurement leads to a value of (4.98 ± 0.1) eV. The reason for this slightly changed value might be a contamination from residual gas adsorption.

Figure 5 depicts the energy dependence of the TPMCD asymmetry for (a) 1PPE and (b) 2PPE. The dashed lines mark the positions of the photoemission thresholds determined from the work-function measurements. In 1PPE as well as in 2PPE the asymmetries are maximum at threshold and drop slightly with increasing photon energy. The relative loss of asymmetry per energy interval is nearly the same for both measurements. However, the absolute asymmetry values differ strongly. In the case of 2PPE a threshold value of 11.7% is detected while for 1PPE only a value of 1.9% is reached. Furthermore, in both cases asymmetry values are observable below the photoemission threshold. Partial band occupation above the Fermi level at 300 K and the spectral width of the laser give reasons for this. The apparent weak oscillation in (a) might be attributed to instabilities in the

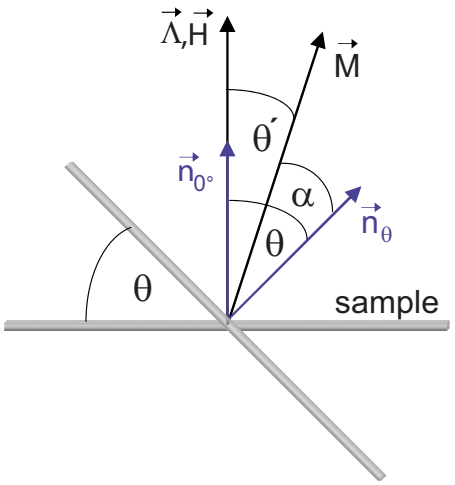

FIG. 6. (Color online) Illustration of the experimental situation within angle-dependent measurements. Rotating the sample by an angle θ results in a sample magnetization $\vec{M}$ oriented under α with respect to the surface normal $\vec{n}$ and under θ' with respect to the photon helicity $\vec{\Lambda}$ and the external magnetic field $\vec{H}$.

generation of the laser light (fourth harmonic) as well as slight differences in the efficiency of the broadband quarter wave plate for different wavelengths. The energy dependence and the different absolute asymmetry values in 1PPE and 2PPE will be discussed later.

For 1PPE at 5.22 eV as well as for 2PPE at 2.46 eV angle-dependent measurements were carried out. Figure 6 illustrates the experimental situation during angle-dependent measurements. The asymmetry is proportional to the scalar product of the helicity vector $\vec{\Lambda}$ of the circularly polarized light and the magnetization vector $\vec{M}$. The directions of the incoming laser light (i.e., the helicity vector $\vec{\Lambda}$) and the external magnetic field $\vec{H}$ stayed parallel ($\vec{\Lambda}\|\vec{H}$). At an angle of incidence of $\theta=0°$, $\vec{\Lambda}$, $\vec{H}$, and $\vec{M}$ are therefore aligned parallel to each other and perpendicular to the sample plane. By rotating the sample by θ, the external field $\vec{H}$ causes the sample magnetization to deviate from the perpendicular orientation. Applying an infinite external field would therefore result in a parallel orientation of $\vec{M}$ and $\vec{H}$. This is not the case for finite external fields. $\vec{M}$ is thus oriented under an angle of θ' with respect to $\vec{H}$. To judge the angle dependence of the asymmetry we therefore have to account for the deviant orientation of $\vec{M}$ with respect to $\vec{H}$ and $\vec{\Lambda}$. This is done by calculating $\theta'=\theta-\alpha$ using the free enthalpy

$$g(\alpha,\theta)=\frac{J_S^2}{2\mu_0}\cos^2(\alpha)+K_1\sin^2(\alpha)+K_{me}\sin^2(\alpha)+\frac{K_S}{t}\cos^2(\alpha)-|\vec{J}_S||\vec{H}|\cos(\theta-\alpha) \quad (2)$$

with the magnetocrystalline anisotropy constant K_1, the anisotropy constant due to magnetoelastic strain K_{me}, and the surface anisotropy constant K_S including both interfaces. The higher order anisotropy term K_2 was neglected. $|\vec{J}_S|=1.8$ T is

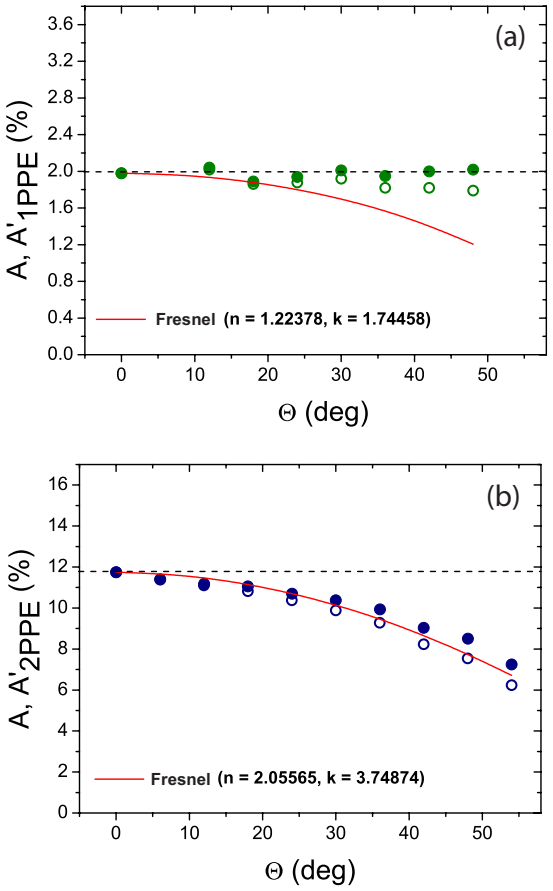

FIG. 7. (Color online) (a) Angle dependence of the 1PPE TPMCD asymmetry measured at a photon energy of 5.22 eV for 4.5 ML Co/Pt(111). (b) Same for 2PPE TPMCD asymmetry measured at a photon energy of 2.46 eV. The open circles show the measured asymmetry values A, the full dots depict the asymmetry values $A'=A/\cos(\theta')$, which account for noncollinear magnetization orientation relative to the photon helicity. The full curves denote the calculations for the relevant MCD creating term $\mathrm{Im}[\cos\vartheta' E'_{\parallel} E'^{*}_{\perp}]$ in the Fresnel-field approximation for 250 nm (1PPE) and 505 nm (2PPE) in Co bulk material.

the magnetization in saturation, $|\vec{H}|=\frac{0.1}{\mu_0}$ T is the applied external field, $t=0.9$ nm is the Co layer thickness, and $\mu_0=4\pi\times10^{-7}$ N A^{-2} is the vacuum permeability. Minimizing $g(\alpha,\theta)$ with respect to α yields

$$\frac{\partial g(\alpha,\theta)}{\partial\alpha}=-2\left[L+\frac{K_S}{t}\right]\cos(\alpha)\sin(\alpha)-|\vec{J}_S||\vec{H}|\sin(\theta-\alpha)=0 \tag{3}$$

with $L=\frac{J_S^2}{2\mu_0}-K_1-K_{me}$, representing the volume energy anisotropy constant. For L a value of 9.2×10^5 J m^{-3} was taken from Ref. 20. The surface anisotropy constant was calculated by using a critical thickness for the spin-reorientation transition of $t_c=1.1$ nm, which was previously detected at a Co wedge on Pt(111). This gives $K_S=-1.01\times10^{-3}$ J m^{-2}. Solving Eq. (3) for α finally yields θ'. Figure 7 shows the angle dependence of the TPMCD asymmetry for 1PPE as well as for 2PPE. The open circles depict the measured asymmetry values, depending on the angle of incidence θ. The full dots represent asymmetry values $A'=A/\cos(\theta')$, taking into account that the magnetization is not collinear with the external field and hence with the photon helicity. While for 1PPE the asymmetry almost stays constant, A' decreases with increasing angle of incidence in the case of 2PPE.

Large angles of incidence normally result in a polarization loss for incoming circularly polarized photons in the sample material. This behavior is well reproduced by the angle-dependent measurements in the case of 2PPE. Moreover, the polarization change also depends on the wavelength of the incoming photons and is therefore different for different photon energies. At first glance, this could be an explanation for the different 1PPE and 2PPE angle dependences. To provide inside into this issue the relevant MCD creating term $\mathrm{Im}[\cos\vartheta' E'_{\parallel} E'^{*}_{\perp}]$ in the Fresnel-field approximation was calculated following Ref. 21, where $E'_{\parallel}$ and $E'_{\perp}$ denote the amplitudes of the electric field components parallel and perpendicular to the plane of incidence inside the material and ϑ' marks the internal polar angle of incidence. This term is equivalent to the loss of circular polarization and is calculated by using the refractive indices for both wavelength (250 nm for 1PPE, 505 nm for 2PPE) in Co bulk material, taken from Ref. 22. Note that for 1PPE a slightly different wavelength compared to the experiment (237.5 nm) has been used, since refractive indices for lower wavelengths are not available in the program code. To allow for comparison with the experiment the calculated values were additionally normalized at $\theta=0°$. While for 2PPE the theory confirms the measurement, the calculation for 1PPE cannot describe the measured constant behavior. Since the calculated polarization loss is, however, almost the same for 1PPE and 2PPE the measured data cannot be explained by the influence of different refractive indices due to different photon energies. A possible reason is the fact that the present theory only holds for bulk materials. However, for 1PPE the existence of a second interface to the substrate might be of greater importance compared to 2PPE because the real parts of the refractive indices of Co and Pt are different in the case of 1PPE while they are almost equal for 2PPE.

IV. DISCUSSION

As outlined above 1PPE as well as 2PPE TPMCD measurements reveal enlarged asymmetries compared to measurements for a capped system. In Ref. 10 a Pt capped Co wedge was grown on a 20 ML Pt buffer layer on W(110). This sample exhibits asymmetry values of 0.06% (1PPE) and 0.10% (2PPE) at 4.5 ML Co thickness. In that case only fixed photon energies of 4.64 eV for 1PPE and 3.1 eV for 2PPE were available. Due to a sample work function of $\Phi=4.6$ eV 1PPE (2PPE) experiments were carried out 0.04 eV (1.6 eV) above threshold. In the case of the uncapped system asymmetries of 1.82% (1PPE) at the same difference between photon energy and sample work function and 8.37% (2PPE) at a maximum difference of 0.86 eV are measured. In both cases the asymmetry values are more than one order of magnitude larger than for the capped system. We briefly recall possible reasons for the reduction in MCD

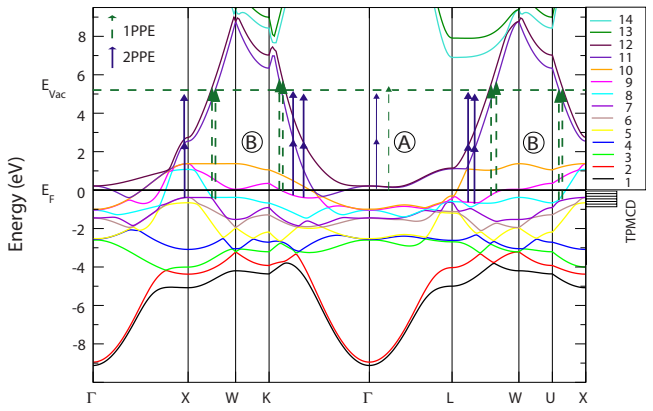

FIG. 8. (Color online) Band structure of fcc Co with a lattice constant of $a=0.35457$ nm. The thin dashed (continuous) arrows denote possible 1PPE (2PPE) transitions in the Γ-L direction (model A) while the bold dashed and continuous arrows show the possible 1PPE and 2PPE excitations in all other crystallographic directions (model B). The hatched region on the right-hand side denotes the energy range of initial bands contributing to 2PPE-TPMCD. The dashed horizontal line indicates the position of the vacuum level E_{Vac} for the 1PPE measurements.

asymmetry values imposed by the capping layer. Photoemission from the Pt cap layer (3 nm thick in Ref. 10) will give a background signal that shows no MCD (except for a possible small polarization of Pt at the interface). Therefore the Pt contribution to the total photoyield will decrease the detected asymmetries. Moreover, the cap layer causes a substantial transport loss of Co photoelectrons, which may depend on the band structure of Pt. These losses do not depend on the photon helicity and will not diminish the MCD of the Co photoelectrons. But they strongly reduce the intensity of the asymmetry-carrying signal. In summary, the transport losses of the Co photoelectrons as well as the extra intensity by the Pt photoelectrons are reasons for the decreased MCD asymmetry.

For the capped as well as for the uncapped system the 2PPE asymmetry is larger than the asymmetry in one-photon photoemission. However, the relative loss of asymmetry per energy interval is nearly the same for 1PPE and 2PPE as shown in Fig. 5. In the following we will analyze this behavior in terms of band-structure calculations. For 2PPE processes the analysis of band transitions is more complicated, since the electrons are excited via a two-step process. The intermediate state can be virtual or real and the selection rules might only apply treating 2PPE as a series of two one-step excitation processes. Moreover, the parity is changed in a one-step process while it does not change in the case of 2PPE.

Relativistic band-structure calculations have been performed on the basis of the local spin-density approximation. Figure 8 shows the calculated energy bands of fcc Co, using a lattice constant of $a=0.35457$ nm, for the low-index crystallographic directions. The dashed horizontal line indicates the vacuum level for 1PPE. The value for 2PPE lies 0.25 eV lower. Vertical arrows denote possible transitions for 1PPE (dashed) and 2PPE (full arrows). Owing to energy conservation only bands located in a narrow region up to 0.61 eV (0.86 eV) below E_F can contribute to the 1PPE (2PPE) signal at the maximum available photon energies. The region for 2PPE has been hatched in Fig. 8, right-hand side. In the presence of spin-orbit coupling the spin as well as the spatial symmetry of the individual bands are no longer good quantum numbers; bandmixing due to hybridization has to be taken into account. Therefore, spin and symmetry character of bands change along the crystallographic directions in a fully relativistic calculation. It is therefore more appropriate to label the bands only with numbers. On the basis of Fig. 8 we consider two possible excitation scenarios A and B.

First we consider usual photoelectron emission from an fcc crystal with (111) surface orientation. In this conventional approach only transitions in the normal emission direction Γ-L of the reciprocal lattice can take place. This is described by model A. At the threshold, normal emission is strictly fulfilled because no excess energy for $k_{\|}\neq 0$ is available. In the regime close to the threshold the escape cone effect limits possible transitions to small $k_{\|}$ values (e.g., $k_{\|_{max}}=0.23$ Å^{-1} at 0.2 eV excess energy). Within model A bands 11 and 12 are good candidates for initial states. Although the calculated bands 11 and 12 in Fig. 8 are located slightly above the Fermi level, epitaxial strain, and /or a possible doping effect of the Pt substrate could shift the actual bands closer to the Fermi level so that they might be occupied at finite temperatures. Photoemission directly at the Fermi edge from the Γ-L direction of fcc Co was also confirmed by Ref. 23. In agreement with former band-structure calculations[24,25] bands 11 and 12 are minority-spin bands in the Γ-L direction and carry *d* character. Note that the band character changes to *sp* type along the L-W and U-X directions, and due to a spin-orbit-induced avoided band-crossing band 11 adopts majority-spin character. Moreover, bands 11 and 12 exhibit large densities of states in the vicinity of the Γ point. However, no final-state band exists in the energy range closely above the vacuum level (dashed horizontal line). Hence, 1PPE electrons are excited to evanescent states, being quasifree continuum states that are strongly damped inside the material (transition marked with thin dashed arrow). In the case of 2PPE the transition along Γ-L can only proceed through a virtual intermediate state to an evanescent final state (thin full arrow). Both the virtual state and the final state carry minority character due to the prohibition of intersystem crossing. In model A the fact that the relative loss of asymmetry per energy interval is similarly small for 1PPE and 2PPE points out that the possible intermediate states in 2PPE might be very similar to each other, influencing the energy dependence of the asymmetry in the same way. Therefore, one might be inclined to think of a "broadband" of virtual intermediate states with similar properties due to lifetime broadening.

In conclusion, model A relies on the fact that only transitions in the Γ-L direction (into evanescent states) are involved in near-threshold photoemission from the (111) face. It thus represents the conventional model of photoemission. In this context, 1PPE spectroscopy measurements on Co/Cu(111) (Ref. 25) reveal the loss of a prominent direct band-to-band transition peak when reducing the photon energy to below 6 eV. However, these measurements did not unambiguously attribute the remaining photoemission intensity to

direct transitions into evanescent states. One argument against scenario A is the fact that the TPMCD asymmetries at least for a Pt-capped Co system are bulk sensitive, i.e., the asymmetry increases with the film thickness up to 8 ML.[10] This finding is highly incompatible with an evanescent final state that is strongly damped inside the material. Concerning 2PPE measurements, model A furthermore lacks an explanation of the enhanced absolute asymmetries compared to 1PPE as there are no real band-to-band transitions accounting for the difference of 1PPE and 2PPE MCD. Since the initial band already carries minority character a spin filter effect of the intermediate state can also be excluded. The fact that 2PPE is a parity-conserving process could be of importance. But apart from this, the enhanced 2PPE asymmetries must be traced back to particular characteristics of the virtual intermediate state which cannot be further determined up to now.

Resuming the conventional interpretation of $k_{\|}$ conserving direct transitions along Γ-L (model A) we are facing several serious discrepancies. The bulk sensitivity of TPMCD as reported previously[10] is in conflict with the missing final-state band. The large difference between the 2PPE and 1PPE MCD asymmetries is at variance with a structureless continuum of virtual intermediate states in the Γ-L direction. We thus search for a possible explanation of the experimental results beyond the conventional direct interband-transition approach. The bulk sensitivity i.e., the increase in MCD up to large thicknesses of 8 ML proves that the relevant final state (or the intermediate state in the 2PPE process) must stem from the bulk band structure. It is thus suggestive to consider directions different from Γ-L, where interband transitions into real final (intermediate) state bands occur. This leads to scenario B.

In scenario B we apply a model that is successfully used for photon-in/photon-out experiments such as the magneto-optical Kerr effect. There, all possible interband transitions in the whole Brillouin zone are considered and the dichroic signal is obtained by averaging over all k directions. This model has proven to be a powerful approach for many different systems.[26,27] We transfer this scenario to our photon-in/electron-out setup with an important modification. In a photoemission process the energy condition (Einstein equation) containing the work function of the material has to be accounted for, i.e., in near-threshold photoemission only a narrow region of initial states below E_F contributes to the observed photoyield. This small region is denoted for the 2PPE case by the hatched area in Fig. 8 in contrast to the much larger area (given by the photon energy) that contributes to MOKE. Energy conservation thus restricts the maximum available binding energy of the initial bands in our case to $E_{B_{\max}}=0.61$ eV (0.86 eV) at the maximum available photon energies for 1PPE (2PPE). Owing to the small photon momentum at the given energies, the electron momentum is conserved during the excitation. For the final emission step additional momentum is needed as discussed later.

In scenario B we thus look for allowed interband transitions in all crystallographic directions with initial bands in the hatched binding energy interval in Fig. 8. Such transitions are marked in Fig. 8 for 1PPE (thick dashed arrows) and for 2PPE (thick full arrows). For the 1PPE case we find interband transitions along Γ-K, U-X and along X-W, L-W. Note, however, that Fig. 8 displays only the projections of the band structure in low-index directions. In the full three-dimensional k space there are many more such transitions in arbitrary k directions. For 2PPE we look for transitions to real intermediate states. Notably, we find 2PPE transitions of this kind close to the X point and in the Γ-K and L-W directions. Most interesting might be the Γ-X direction, since the transition takes place in the vicinity of the high-symmetry X point. Bands 6 and 7 carrying a high density of states in the vicinity of X serve as initial states. Bands 11 and 12 also exhibit a high density of states at X pointing at high transition probabilities. In all cases the final state for 2PPE is again an evanescent state.

1PPE and 2PPE processes are restricted to the mentioned transitions as long as lifetime broadening of the intermediate and final states is not regarded. Otherwise, also excitations from other initial bands might be involved depending on the magnitude of the lifetime broadening.

For reasons of clarity Fig. 8 shows only the high-symmetry directions. The following calculations, however, are performed taking into account all crystallographic directions and obeying energy conservation. This means that k is integrated over the whole Brillouin zone.

To check the validity of model B, we have performed *ab initio* calculations of the TPMCD. The appropriate theoretical formalism for deriving magnetic dichroic spectra is relativistic energy-band theory combined with the linear-response theory to treat the magneto-optical response of the material (see, e.g., Ref. 26). We adopt this formalism to model first the optical excitation in the material due to the incident laser light. In a magnetic material with polar magnetization configuration ($\vec{M}\|\vec{z}$), the wavelength-dependent refractive indices for right (−) and left (+) circularly polarized light traversing the material are given by $n_{\pm}^2=\varepsilon_{xx}\pm i\varepsilon_{xy}$, where ε_{xx} and ε_{xy} are components of the permittivity tensor $\boldsymbol{\varepsilon}$. The latter tensor is related to the optical conductivity tensor, $\boldsymbol{\sigma}$, through $\varepsilon_{ij}=\delta_{ij}+4\pi\sigma_{ij}/\omega$. $\boldsymbol{\sigma}$ can be computed within the linear-response formalism. To treat, however, the 1PPE and 2PPE processes appropriately, additional assumptions must be made and constraints on the excitation must be included. The TPMCD can be approximated by assuming that the intensity of the created photoelectrons I_e is directly proportional to the intensity of the light absorbed in the medium I_{abs}. This approximation is the common assumption underlying electron-yield detection of x-ray dichroism.[28,29] In normal incidence the intensity of created photoelectrons is hence given by $I_e^{\pm}\propto I_{abs}^{\pm}=I_0[1-\exp(-\mu^{\pm}d)]$, where I_0 is the intensity of the incoming radiation, d is the depth in the material, and $\mu^{\pm}$ is the absorption coefficient for left, respectively, right circularly polarized light. The absorption coefficient is connected to the refractive index through $\mu^{\pm}=-2\omega\,\mathrm{Im}[n^{\pm}]/c$. Once $n^{\pm}$ has been obtained from the computed conductivity tensor $\boldsymbol{\sigma}$, it is straightforward to evaluate the corresponding electron intensities $I_e^{\pm}$ and from these the TPMCD asymmetry using Eq. (1) for the case of reversed photon helicity.

As a next step we consider the conditions for the specific 1PPE or 2PPE excitation process that are to be included in the calculations of the $\boldsymbol{\sigma}(\omega)$ tensor. To start with, we note

that in the *ab initio* approach only transitions to real bands are accounted for, excitations to evanescent or virtual states are not regarded. In the light of the above discussion, this implies that the excitation process for 1PPE can be fully described while for 2PPE only the first excitation step into a real intermediate state can be treated.

The 1PPE process is comparably easy to model. The escape of created photoelectrons requires their band energy to be equal or larger than the work function. Hence, in the linear-response expression for σ_{ij} the sum over occupied initial states and unoccupied final states (see, e.g., Ref. 30) consists of only those final states with energies above the work function ($\epsilon_{\text{final}} \geq \Phi$). Also, as mentioned before the maximum photon energy used in the experiment restricts the possible initial states [$\epsilon_{\text{init}} \geq -(h\nu_{\max} - \Phi)$].

2PPE TPMCD is not yet well understood and its modeling requires further assumptions. A model treatment for 2PPE TPMCD has recently been discussed in Ref. 9. In this paper two approaches were considered: one in which the 2PPE consists of two unconnected 1PPE excitation steps and a second one in which there is a coherent, simultaneous absorption of two photons. The latter approach was preferred in the previous study;[9] for ternary Heusler alloys it gave theoretical 2PPE TPMCD asymmetries, which were in good agreement with the measured values. In this work we have also tested the second way of computing 2PPE TPMCD on fcc Co. This gives 2PPE TPMCD values of the same order of magnitude as the 1PPE TPMCD, but it does not reproduce the measured values of about 10%. This finding is understandable because, in contrast to the Heusler alloys, there are only two real final bands available in fcc Co at 5 eV above E_F (see Fig. 8). As mentioned above, this suggests the involvement of an evanescent final state instead of a real band state. The first part of the 2PPE process with a transition to a real intermediate state can, however, be treated with *ab initio* calculations, assuming similar conditions as above for 1PPE but for $\Phi_{2\text{PPE}}/2$ and corresponding photon energies.

We start our discussion of the calculated results with first considering the 1PPE process. Figure 9 shows a spin-resolved calculation of the imaginary and real parts of the conductivities σ_{xy} and σ_{xx} for the 1PPE excitation as a function of photon energy. The dashed curve gives the conductivity spectra due to majority-spin excitations, the full curve those due to minority-spin transitions. A work function of 4.9 eV is used while a typical lifetime broadening of 0.4 eV of the final state is assumed, which is equivalent to a softening of the energy condition for the maximum accessible binding energy. As a result, the absorptive parts of the spectra (Re[σ_{xx}] and Im[σ_{xy}]) increase steeply around the work-function value. The tail at energies $\leq\Phi$ is due to lifetime broadening effects. The dispersive parts of the spectra (Im[σ_{xx}] and Re[σ_{xy}]) can, of course, extend farther to lower energies. The calculations reveal a strong asymmetry in the majority-spin and minority-spin contributions, particularly in the energy range of interest, 5–6 eV.

In Fig. 10 we show several computed 1PPE TPMCD spectra. The calculated TPMCD varies around 1%, which is about a factor of two smaller than the experimental values (dots). Toward the threshold the computed asymmetry falls off whereas the experimental counterpart shows a slight increase. The behavior near the threshold in the calculations is related to how the conditions on the initial and final band energies are enforced. This means that depending on the choice and the sharpness of the experimental parameters (maximum binding energy, work function, lifetime broadening), which are not exactly known, the calculated energy dependence can change toward a better agreement with the measured trend of the MCD asymmetry. For Fig. 10 we have used reasonable values for the lifetime broadening that showed good results for MOKE. One probable reason for the drop of the experimental values with increasing photon energy is that there is an increasing underlying background signal of secondary electrons that does not show an MCD. The reasonable correspondence in the magnitude of the calculated and measured 1PPE TPMCD prompts that the basic mechanism for the 1PPE is the influence of spin-exchange

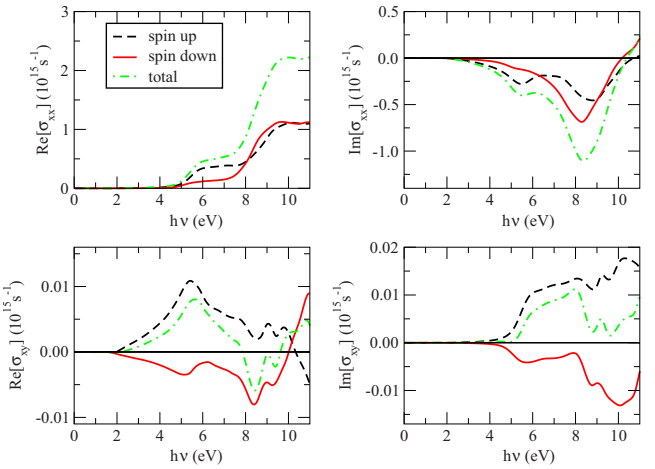

FIG. 9. (Color online) Calculated spin-resolved 1PPE optical conductivity spectra. Shown are the imaginary and real parts of σ_{xy} and σ_{xx} for 1PPE as a function of photon energy. A work function of 4.9 eV and a lifetime broadening of 0.4 eV are used.

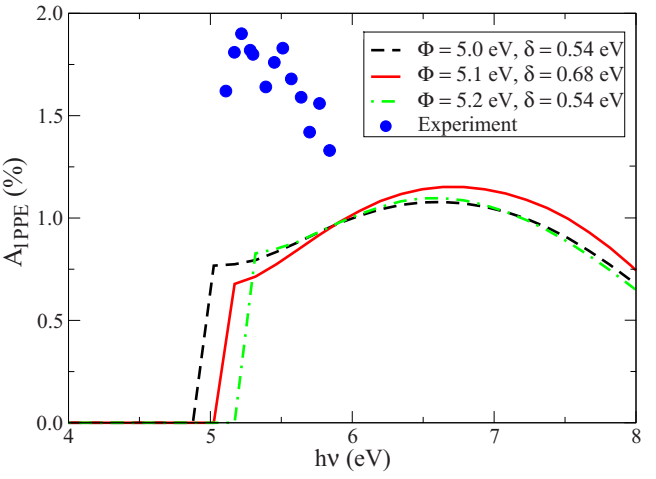

FIG. 10. (Color online) 1PPE TPMCD spectra of fcc Co, computed for different work functions Φ and lifetime broadenings δ. The points represent the measured data.

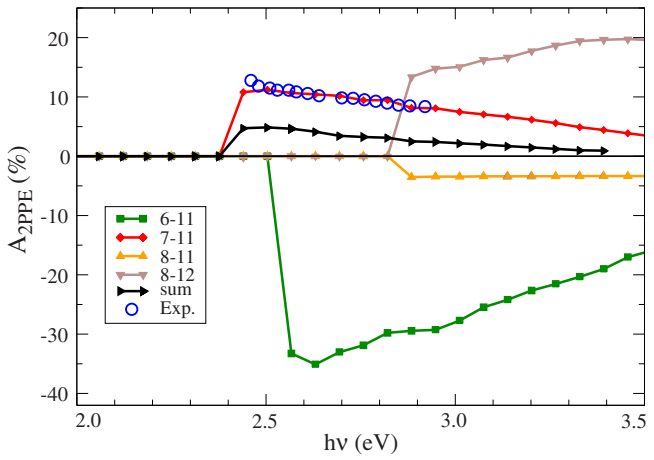

FIG. 11. (Color online) Simulation of the TPMCD for the first excitation step in a 2PPE process. Shown are the calculated TPMCD spectra of fcc Co due to several pertinent band transitions. A work function of 2.49 eV and a lifetime broadening of 0.4 eV are assumed. The resulting MCD of all bands is reduced to 5%. Values below 2.4 eV have been set to zero because of numerical errors due to small emission intensities.

and spin-orbit interactions on the single-particle energy bands. These interactions are quite well captured by relativistic band-structure theory.

As mentioned above, for 2PPE especially excitations in the vicinity of the X point are of interest. We have computed the first step of the 2PPE excitation process investigating the real interband transitions in the photon energy range of $h\nu = \Phi_{2PPE}/2 = 2.49$ eV up to $h\nu_{max} = 2.92$ eV. High TPMCD asymmetries result from the transitions of bands 6 and 7 to band 11 and 8 to 12 near X. In Fig. 11 we show the computed TPMCD of the corresponding excitation channels, calculated through k integration over the whole Brillouin zone. The computed MCD values for individual interband transitions are much larger than the total 1PPE MCD shown in Fig. 10, calculated by summing over all bands. Especially the transitions $6 \rightarrow 11$, $7 \rightarrow 11$, and $8 \rightarrow 12$ give maximal MCD values of −33%, 10%, and 14%, respectively. The onset of the $8 \rightarrow 12$ (and also $8 \rightarrow 11$) transition is, however, just at 2.9 eV, i.e., at the end of the experimentally probed range, therefore these transitions contribute little to the experimental signal. The MCD spectrum is dominated by the $7 \rightarrow 11$ transition. Although $6 \rightarrow 11$ gives a large MCD signal when computed for the single band-to-band transition (squares), it's contribution is heavily reduced when summed up with other transitions. The resulting MCD of all bands (lying triangels) is reduced to 5%, which is a factor of two smaller than the experimental 2PPE MCD values. Since it is dominated by the $7 \rightarrow 11$ transition it also exhibits the same energy dependence. Due to contributions from all other allowed band-to-band transitions to σ_{xx} the total asymmetry is, however, smaller. The relative energy dependence of the experimental data is also well reproduced by theory.

The calculation validates that specific band-to-band transitions (in the vicinity of high-symmetry points) are very likely the source of the large 2PPE MCD. Through the rather narrow accessible energy range of 2.49–2.92 eV, mainly the $7 \rightarrow 11$ transition channel dictates the first step of the 2PPE excitation. Assuming that the TPMCD would not be significantly altered in the second excitation step to an evanescent final state, the resulting 2PPE TPMCD would be on the order of 5% and, hence, larger than the 1PPE TPMCD. More generally, one can conclude that large asymmetry values in the near threshold yield could be triggered by specific band-to-band transitions and that the first excitation step might be the major asymmetry-creating process. In summary, the model applied in scenario B yields agreement within a factor of 2 with the measured MCD asymmetries. Moreover, the factor of 6 between the 2PPE and 1PPE asymmetries is well reproduced by theory. We thus propose the explanation that indeed interband transitions in other directions than Γ-L are responsible for the large MCD measured for Co films on Pt(111).

In view of the encouraging agreement, we continue this nonconventional model and search for a mechanism that allows a (probably small) fraction of these electrons with $k_{\parallel} \neq 0$ to surmount the surface barrier. When irradiating the Co film with near-threshold photons, we induce direct interband transitions in different k directions. Near-threshold excitation therefore creates many hot electrons in band states in various k directions inside of the material. The energy of these excited electrons is sufficient to overcome the surface barrier (all arrows in Fig. 8 end at or above E_{Vac}). However, their k-vectors point in various directions away from the surface normal. Therefore additional momentum has to be transferred to the electron. Bulk or surface Umklapp processes adding a reciprocal lattice vector to the k vector, is ruled out at such low kinetic energies. Consequently, only scattering processes with momentum transfer can serve as assisting mechanisms. In electron-electron scattering the total energy is shared between the two interacting electrons. However, any energy loss of the photoexcited electron ends up in a state below E_{Vac} so that the electron cannot escape from the surface. Electron-phonon and accordingly electron-magnon scattering are thus left as the final possibilities. Since phonons/magnons carry large momenta but small energies a quasielastic scattering with a low-frequency phonon/magnon can transfer enough momentum to the electron to escape into vacuum. Note that in electron-magnon scattering the spin of the electron is reversed, for electron-phonon scattering this is mostly not the case. Since the present measurement technique is not sensitive to the spin of the escaping electron the two processes cannot be distinguished. In normal photoemission experiments these weak contributions are masked by the strong direct interband transitions. However, in our case no direct interband transitions in Γ-L are possible so that the phonon/magnon-assisted processes become significant in the near-threshold photoyield and, hence, for the TPMCD.

Finally, the calculations in Fig. 11 demonstrate that the existence of a real intermediate state in the 2PPE transition is of great importance for the high TPMCD asymmetry to occur. In model A the intermediate state can only be virtual and we have no further information except that its pure existence should somehow cause a strongly enhanced 2PPE asymmetry. The resonant interband transition in model B, however, allows for quantitative conclusions. The excitation to a real intermediate state is not only favorable since the dipole ma-

trix element between two real states is large and the two-step process will proceed very effectively. Also the enhanced lifetimes of real states cause a large mean free path of the electrons. This explains the large probing depth (bulk sensitivity) and directly increases the possibility for an electron-phonon interaction.

The calculations have shed light into the question, why for the fcc Co-film the 2PPE asymmetries are six times larger than 1PPE asymmetries, which is different from the case of Ni(100).[11] For 1PPE the electron-phonon interaction must take place after the outright excitation of the electron into a real final state. For 2PPE the scattering process could happen either after the excitation to the real intermediate state or after the whole two-step process. The first possibility causes an increase in the electron-phonon scattering probability. In this sense, time-resolved measurements would be interesting and helpful to investigate whether scattering already appears in the intermediate state or the electron is first excited via the two-step process to the final state before it interacts with a phonon. However, those experiments would require pulse widths in the few-femtosecond range.[31]

For the given band structure of fcc Co and photon energy range, most relevant 2PPE transitions showing high MCD asymmetries can be found around the X point. Although not only the low-index crystallographic directions contribute to the signal and k is integrated over the whole Brillouin zone, this observation suggests that transitions in the vicinity of high-symmetry points in k space might be favorable for large dichroic signals. Furthermore, the slope of the bands involved in the emission process plays a crucial role. Flat band regions like those of the initial bands 6 and 7 and the real intermediate bands 11 and 12 exhibit large densities of states and thus give rise to high partial intensities.

For 1PPE as well as for 2PPE the measured asymmetries are a factor of 2 larger than the calculated values. A reason for this might be a selection mechanism in the phonon-scattering process. In theory all k directions are averaged equally. In the experiment scattering with lower momentum transfer is more probable than phonon scattering with higher momentum transfer. This would be advantageous for k vectors with higher projection onto the surface normal against those with low projection.

V. CONCLUSION

Energy- and angle-dependent magnetic circular dichroism measurements in threshold photoemission (TPMCD) for one- and two-photon photoemission (1PPE and 2PPE) have been carried out on a 4.5 ML Co film on Pt(111). The fourth and second harmonic of a femtosecond laser served as photon source yielding $h\nu=(5.06-5.84)$ eV and $h\nu=(2.49-2.92)$ eV for 1PPE and 2PPE, respectively.

Energy-dependent measurements reveal maximum asymmetries directly at the photoemission threshold (1.9% for 1PPE and 11.7% for 2PPE) that weakly decrease with increasing photon energy. A fully relativistic band-structure calculation for fcc Co provides the basis for quantitative comparison of the magnetic asymmetries. Since for the normal-emission direction (i.e., Γ-L) there is neither a real final state nor a real intermediate state for 2PPE the standard model of direct interband transitions cannot be applied to near-threshold photoemission from fcc Co(111) and, likewise, not for hcp Co(0001).[23] Instead, we have treated the problem analogously to MOKE theory with the additional restriction in energy due to the existence of the sample work function in the energy equation of the photoemission process. The latter leads to a narrow energy interval of initial states, in our case only 0.86 eV (2PPE) and 0.61 eV (1PPE) below E_F for the maximum photon energies used. In the case of 1PPE the calculations are in reasonable agreement with the measured TPMCD responses which emphasizes that the origin of the 1PPE magnetodichroic effect is the combined influence of the exchange splitting and spin-orbit interaction on single-particle energy bands. For 2PPE only the first excitation step could be simulated due to the lack of a real final state. Here, the existence of a real intermediate state is of great importance and the enlarged 2PPE asymmetry is mainly attributed to specific interband transitions between initial and intermediate states. Also the prevailing appearance of transitions between bands, carrying a high density of states in the vicinity of a high-symmetry point in k space gives reasons for the enhanced-asymmetry values. As the relevant transitions occur in crystallographic directions other than Γ-L, additional momentum has to be delivered by a secondary process. We propose electron-phonon and/or electron-magnon scattering processes as assisting mechanism.

Angle-dependent measurements reveal a constant asymmetry in the case of 1PPE that might be explained by the presence of a second (Co/Pt) interface. For 2PPE the asymmetry decreases with increasing angle of incidence. This behavior could be quantitatively modeled using the Fresnel formalism leading to a loss of circular polarization in bulk material with increasing angle of incidence. In this case the second interface has no effect due to the equal refraction indices of Co and Pt. The measurements also demonstrate that large angles of incidence as used in standard photoemission electron microscopy setups are still sufficient to exploit large dichroic effects as magnetic contrast mechanism.

In conclusion the measurements on Co films on Pt(111) demonstrate that a sizeable TPMCD can be measured even in cases where no special band-structure features as in the case of Ni (spin-orbit split band close to E_F) are present and even band-to-band transitions in conventional normal electron emission (Γ-L direction) are not possible. Unlike the case of Ni(001),[11] the asymmetry is almost energy independent and still large for photon energies 0.5 eV above threshold with enhanced electron intensities so that a fine tuning of the photon energy is not needed in this case. Our experiments demonstrate that unique band-structure features are not necessarily required. Although shown for the specific example of Co(111), the present results give evidence that sizeable asymmetry values can be expected for many more materials.

For detecting large asymmetry values in future experiments it would be advantageous to first inspect the band structure of suitable materials considering the available photon-energy range, work function, and crystallographic direction. With the knowledge of the present work, resonant

transitions to real intermediate bands (in the case of 2PPE) or real final bands (in the case of 1PPE) would be promising candidates for large asymmetry signals. The transitions must not necessarily occur along the direction of observation, since phonon or magnon scattering can provide the necessary momentum transfer in near-threshold yield experiments. The transitions should preferably be located in the vicinity of high-symmetry points in k space with participating bands carrying high density of states and predominantly one-spin character. These criteria will allow for a direct tailoring of TPMCD asymmetries in future experiments.

ACKNOWLEDGMENTS

This work was supported by the Carl-Zeiss-Stiftung and the Graduate School Materials Science in Mainz (Kerstin Hild), by Deutsche Forschungsgemeinschaft (Grant No. EL 172/15-1), by the Grant-in-Aid for Scientific Research from JSPS (Grants No. 19201023 and No. 19681013) and the IMS International Program, by the Swedish Research Council, the C. Tryggers Foundation, and the Swedish National Infrastructure for Computing (SNIC). Furthermore the authors would like to thank G. H. Fecher and W. Kuch for fruitful discussions.

*hildk@uni-mainz.de

[1] G. Schütz, W. Wagner, W. Wilhelm, P. Kienle, R. Zeller, R. Frahm, and G. Materlik, Phys. Rev. Lett. **58**, 737 (1987).
[2] B. T. Thole, P. Carra, F. Sette, and G. van der Laan, Phys. Rev. Lett. **68**, 1943 (1992).
[3] P. Carra, B. T. Thole, M. Altarelli, and X. Wang, Phys. Rev. Lett. **70**, 694 (1993).
[4] J. Stöhr, J. Magn. Magn. Mater. **200**, 470 (1999).
[5] G. K. L. Marx, H. J. Elmers, and G. Schönhense, Phys. Rev. Lett. **84**, 5888 (2000).
[6] T. Nakagawa and T. Yokoyama, Phys. Rev. Lett. **96**, 237402 (2006).
[7] T. Nakagawa, T. Yokoyama, T. Hosaka, and M. Katoh, Rev. Sci. Instrum. **78**, 023907 (2007).
[8] K. Hild, J. Maul, T. Meng, M. Kallmayer, G. Schönhense, H. J. Elmers, R. Ramos, S. K. Arora, and I. V. Shvets, J. Phys.: Condens. Matter **20**, 235218 (2008).
[9] K. Hild, J. Maul, G. Schönhense, H. J. Elmers, M. Amft, and P. M. Oppeneer, Phys. Rev. Lett. **102**, 057207 (2009).
[10] K. Hild, J. Emmel, G. Schönhense, and H. J. Elmers, Phys. Rev. B **80**, 224426 (2009).
[11] T. Nakagawa, I. Yamamoto, Y. Takagi, K. Watanabe, Y. Matsumoto, and T. Yokoyama, Phys. Rev. B **79**, 172404 (2009).
[12] W. B. Zeper, F. J. A. M. Greidanus, P. F. Carcia, and C. R. Fincher, J. Appl. Phys. **65**, 4971 (1989).
[13] S. C. Shin, Appl. Surf. Sci. **65-66**, 110 (1993).
[14] N. W. E. McGee, M. T. Johnson, J. J. de Vries, and J. aan de Stegge, J. Appl. Phys. **73**, 3418 (1993).
[15] P. M. Oppeneer, J. Sticht, T. Maurer, and J. Kübler, Z. Phys. B: Condens. Matter **88**, 309 (1992).
[16] P. M. Oppeneer, V. N. Antonov, T. Kraft, H. Eschrig, A. N. Yaresko, and A. Y. Perlov, J. Phys.: Condens. Matter **8**, 5769 (1996).
[17] C. S. Shern, J. S. Tsay, H. Y. Her, Y. E. Wu, and R. H. Chen, Surf. Sci. **429**, L497 (1999).
[18] U. Gradmann and G. Waller, Surf. Sci. **116**, 539 (1982).
[19] E. Lundgren, B. Stanka, M. Schmid, and P. Varga, Phys. Rev. B **62**, 2843 (2000).
[20] C.-J. Lin, G. L. Gorman, C. H. Lee, R. F. C. Farrow, E. E. Marinero, H. V. Do, H. Notarys, and C. J. Chien, J. Magn. Magn. Mater. **93**, 194 (1991).
[21] J. Henk and R. Feder, Phys. Rev. B **55**, 11476 (1997).
[22] M. Polyanskiy, Refractive index data base, http://refractiveindex.info
[23] F. J. Himpsel and D. E. Eastman, Phys. Rev. B **21**, 3207 (1980).
[24] M. Pickel, A. B. Schmidt, F. Giesen, J. Braun, J. Minár, H. Ebert, M. Donath, and M. Weinelt, Phys. Rev. Lett. **101**, 066402 (2008).
[25] W. Kuch, A. Dittschar, M. Salvietti, M.-T. Lin, M. Zharnikov, C. M. Schneider, J. Camarero, J. J. de Miguel, R. Miranda, and J. Kirschner, Phys. Rev. B **57**, 5340 (1998).
[26] P. M. Oppeneer, in *Handbook of Magnetic Materials*, edited by K. H. J. Buschow (Elsevier, Amsterdam, 2001), Vol. 13, pp. 229–422.
[27] H. Ebert, Rep. Prog. Phys. **59**, 1665 (1996).
[28] S. Hüfner, *Photoelectron Spectroscopy* (Springer, Berlin, 2003).
[29] R. Nakajima, J. Stöhr, and Y. U. Idzerda, Phys. Rev. B **59**, 6421 (1999).
[30] P. M. Oppeneer, T. Maurer, J. Sticht, and J. Kübler, Phys. Rev. B **45**, 10924 (1992).
[31] M. Aeschlimann, M. Bauer, S. Pawlik, W. Weber, R. Burgermeister, D. Oberli, and H. C. Siegmann, Phys. Rev. Lett. **79**, 5158 (1997).